mater.scichina.com link.springer.com

Published online 29 October 2021 | https://doi.org/10.1007/s40843-021-1800-0
Sci China Mater 2022, 65(4): 1020–1027

Precise synthesis of multilevel branched organic microwires for optical signal processing in the near infrared region

Chang-Cun Yan[1], Jun-Jie Wu[1], Wan-Ying Yang[1], Song Chen[1], Qiang Lv[1], Xue-Dong Wang[1*] and Liang-Sheng Liao[1,2*]

ABSTRACT **Complicated multilevel micro/nanostructures have attracted great attention as essential basic components of integrated optoelectronic devices. However, precise synthesis of these well-designed micro/nanostructures is still a major challenge. In this report, a series of near-infrared emissive multilevel branched organic microwires with different integrated levels are successfully fabricated for the first time by a facile self-assembly approach based on our well designed and synthesized (2*E*,2′*E*)-1,1′-(1,5-dihydroxynaphthalene-2,6-diyl)bis(3-(4-(dimethylamino)phenyl)prop-2-en-1-one) (DHNBP). The growth mechanism is attributed to lattice matching between (100) and (010) crystal planes, with an interplanar spacing mismatch rate as low as 5.3%. Benefiting from the uniaxial oriented molecular packing mode of the crystal, the well-prepared microwires have outstanding optical properties. More significantly, the branched structures can work as optical logic gates and optical signal processors. Therefore, this synthesis method for multilevel branched microwires will potentially facilitate the development of organic integrated optoelectronics.**

Keywords: organic homostructure, solution self-assembly, lattice matching, asymmetric optical waveguide, integrated photonics

INTRODUCTION

Integrated electronic chips with electrons as information carriers are approaching their inherent limit caused by interconnect delays and heat generation [1]. In comparison, photons have intrinsically higher information-carrying capacity and produce a low heat load [2]. Therefore, photonic chips based on integrated optical circuits with photons as information carriers are attracting more attention and are considered to be ideal substitutes for their electronic counterparts [3–5]. To achieve this end, a toolbox of micro or nano scale optical components based on micro/nanowires have been developed, such as light emitting diodes [6,7], lasers [8,9], optical waveguides [10], field effect transistors (FETs) [11,12], and all-optical switches [13,14]. Nevertheless, the fabrication of integrated multilevel microstructures with advantages over individual micro/nanowires in optical circuits remains a major challenge. Moreover, most of the reported multilevel micro/nanowires have been fabricated based on inorganic semiconductor materials through lithography [15,16] and micromanipulation [17,18]. These are complicated techniques that could cause poor stability and severe optical loss because of simple physical interaction at the junction position with a nonnegligible lattice mismatch.

Compared with their inorganic counterparts, organic semiconductor materials are more attractive for photonic applications due to their large optical cross-sections, tailorability of molecular structures, broad spectral tunability, and solution-based processing ability [19]. Besides, organic materials can easily self-assemble into micro/nanocrystals based on weak intermolecular interactions, such as the van der Waals interaction, π-π interaction, and hydrogen/halogen bonds, with nearly negligible lattice mismatch that enables the realization of organic FETs [20–22], organic optical waveguides [23,24], and organic solid-state lasers [25–28]. In recent decades, organic micro-hetero/homostructures, like multiblock structures [29], core-shell structures [30–32], branched structures [33–35], and multilevel structures [36,37], have been developed by our group and others *via* the self-assembly method. Among these structures, branched micro/nanowires have drawn much attention because branching can naturally achieve parallel connectivity and interconnection, which are essential to functional logic gates for data computing [38]. For example, Zhao and coworkers [39–41] developed a series of branched microwires that included dendritic heterostructures, organic/metal hybrid branched heterostructures, and H-type organic microwires that could be used for optical signal manipulation. Later, Fu and coworkers [42] also reported H-type organic branched microwires with two components, which demonstrated the functions of a multi-channel signal converter and laser-power meter system. Branched organic homostructures can also work as optical logic gates and wavelength division multiplexing systems because of the asymmetrical waveguide property at the junction position [43,44]. However, most reported branched structures are primary branched structures in which one or more micro/nanowires grow in the side direction from a backbone. Higher integrated branched structures, such as secondary or multilevel branched structures (Fig. 1a), in which one or more micro/nanowires grow in the side direction from a branch, can provide more complex optical logic operation possibilities. However, the fabrication of this kind of structure is still a challenge.

Nowadays, near-infrared (NIR) emissive organic materials are receiving more attention for their potential applications in tel-

[1] Institute of Functional Nano & Soft Materials (FUNSOM), Jiangsu Key Laboratory for Carbon-Based Functional Materials & Devices, Soochow University, Suzhou 215123, China
[2] Macao Institute of Materials Science and Engineering, Macau University of Science and Technology, Taipa 999078, Macau SAR, China
* Corresponding authors (emails: wangxuedong@suda.edu.cn (Wang XD); lsliao@suda.edu.cn (Liao LS))

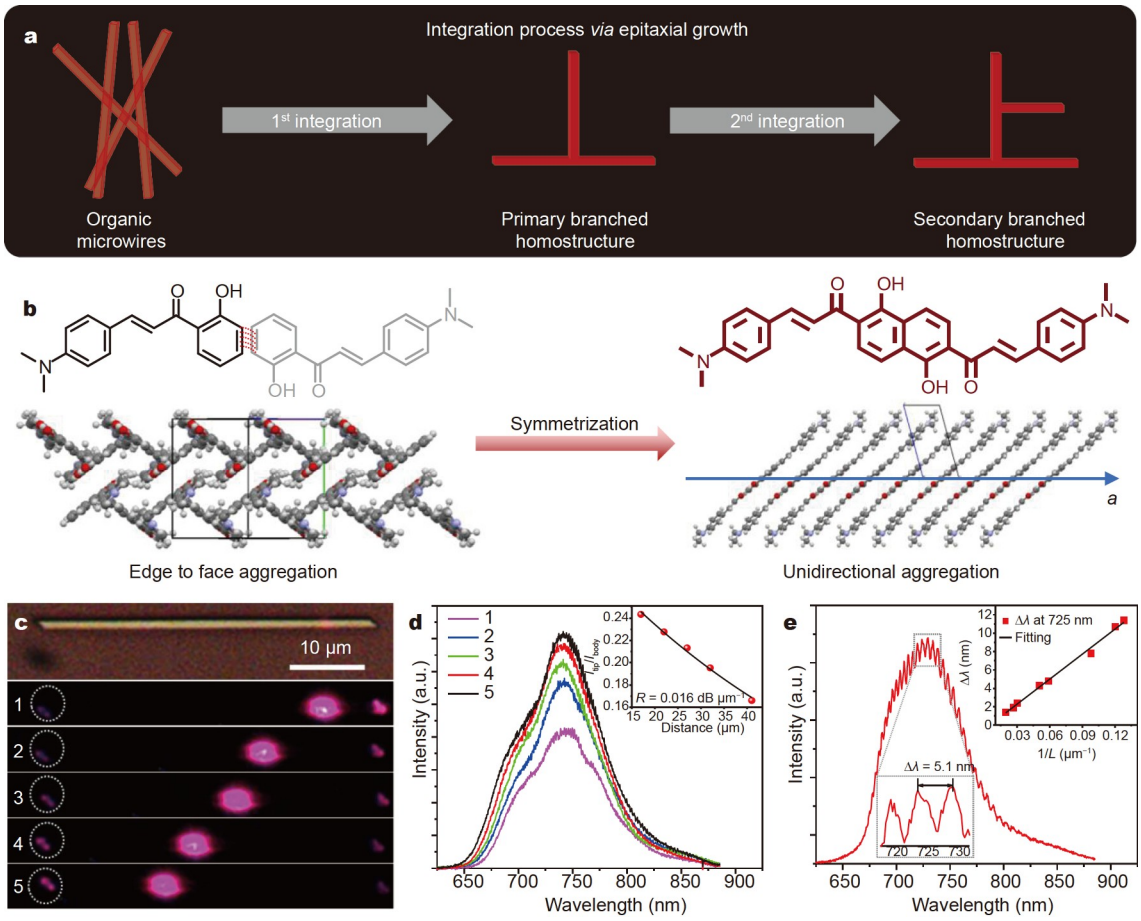

Figure 1 (a) Schematic of the integration process of multilevel microwires *via* epitaxial growth. (b) Molecular structures and packing structures of DHMAC and DHNBP crystals. (c) Bright-field microscopy image and photoluminescence (PL) microscopy images of an individual microwire excited with a focused laser beam (λ = 375 nm) at different positions. (d) Corresponding PL spectra at positions 1–5. Inset: related curve of the ratio between the PL intensity at 740 nm at the tip and excitation position (I_{tip}/I_{body}) *versus* the distance between the tip and the excitation position (D). The curve was fitted by an exponential decay function ($I_{tip}/I_{body} = A\exp(-RD)$). (e) PL spectrum of a 17.5-μm-long microwire and partial magnification at a wavelength of 725 nm. Inset: related curve of the space between resonance peaks ($\Delta\lambda$) at 725 nm *versus* $1/L$ (L: microwire length). The curve was fitted by a linear function.

ecommunications [45,46], bioimaging [47,48], night-vision target identification [49], information security displays [50], and sensors [51]. In integrated optical devices, long wavelength emission can help decrease the optical loss caused by Rayleigh scattering in an optical waveguide [46]. However, organic molecules with NIR emission are highly limited, let alone NIR-branched microwires. Herein, for the first time, we have successfully synthesized NIR emissive multilevel branched microwires made of (2*E*,2′*E*)-1,1′-(1,5-dihydroxynaphthalene-2,6-diyl)bis(3-(4-(dimethylamino)phenyl)prop-2-en-1-one) (DHNBP) using a facile solution-evaporation method. DHNBP forms individual microwires at good-solvent-dominated conditions, while it forms branched structures at poor-solvent-dominated conditions. Sequentially, the growth mechanism of the branched structures was investigated, and it was determined that lattice matching plays an important role in the formation of branch structures and that supersaturation affects the final branch morphologies. We demonstrated that DHNBP molecules are packed in a uniaxially oriented mode in the crystalline state, which endows the microwires with outstanding optical properties, such as excellent optical waveguide performance, resonator effect, and high polarized emission. The branched microwires also showed interesting optical waveguide properties, which suggest that they can function as photonic components. The primary branched structures showed different cavity effects at the trunk and branch regions: acting as an asymmetric optical waveguide at the truncation position and exhibiting a polarized-light propagation property. Significantly, the secondary branched microwires integrate two branched structures together at different levels. The function of the secondary branched microwires as a combined signal processor is also exhibited in this study. Overall, our study provides new multilevel branched organic microwires with different aggregation levels that can potentially be used as photonic components in integrated optical circuits.

EXPERIMENTAL SECTION

General information

All reagents and solvents were used as received and without further purification, except for tetrahydrofuran (THF). THF was dried by distillation from sodium/benzophenone under nitrogen. ^{1}H nuclear magnetic resonance (NMR) and ^{13}C NMR spectra were measured on a Bruker 400-MHz spectrometer at 298 K with chemical shifts (δ, ppm) relative to tetramethylsilane (Me_4Si). High-resolution mass spectra were measured on a

Waters GCT Premier mass spectrometer. Field-emission scanning electron microscopy (FESEM) images of the samples were observed using an FESEM (Carl Zeiss, Supra 55) at an acceleration voltage of 10 kV. Transmission electron microscopy (TEM) images were obtained using a TEM (FEI company, Tecnai G2 F20, United States). For TEM measurements, one drop of solution was dropped on a carbon-coated copper grid and evaporated at room temperature. TEM measurements were performed at an accelerating voltage of 100 kV. X-ray diffraction (XRD) patterns were measured using a D/max 2400 X-ray diffractometer with Cu Kα radiation (λ = 1.54050 Å). Steady-state fluorescence spectra of the samples were measured using a HITACHI F-4600 fluorescence spectrophotometer. Fluorescence microscopy images were obtained using a Leica DMRBE fluorescence microscope with a spot-enhanced charge couple device (CCD, Diagnostic Instrument, Inc.). Samples were prepared for optical characterization by placing a drop of dispersion onto a cleaned glass slide. Microarea photoluminescence (μ-PL) spectra were collected on a homemade optical microscope. To measure the photoluminescence (PL) spectra of individual microwires, a microwire was excited locally with a 375-nm laser focused down to the diffraction limit. The excitation laser was filtered with a 375-nm notch filter. The light was subsequently coupled to a grating spectrometer (Princeton Instrument, ARC-SP-2356) and recorded by a thermal-electrically cooled CCD (Princeton Instruments, PIX-256E). PL microscopy images were taken with an inverted microscope (Olympus, BX43).

Synthesis of DHNBP

The synthesis method and characterization of DHNBP and intermediate compounds are detailed in the Supplementary information (Scheme S1, Figs S1–S4).

Single-crystal information

Single-crystal DHNBP was obtained by the solvent vapor evaporation method. First, 2 mg DHNBP was dissolved in 4 mL dichloromethane (DCM) and then 2 mL EtOH was carefully added. DHNBP single crystals were obtained after most of the solvent evaporated. Single-crystal XRD data were collected on a Bruker D8-Venture diffractometer with a Turbo X-ray Source (Mo-Kα radiation, λ = 0.71073 Å), adopting the direct drive rotating anode technique and a CMOS detector at room temperature. The data frames were collected using the APEX2 program and processed using the program SAINT routine in APEX2. Structures were solved by direct methods and refined by the full-matrix least squares on F2 using the SHELXTL-2014 program. Crystallographic data were compared with the Cambridge Crystallographic Data Center supplementary publication no. CCDC-2081135 (DHNBP).

Fabrication of DHNBP microwires

Organic DHNBP microwires were prepared by a facile solution–evaporation method using mixed DCM and EtOH. During the preparation process, 1 mg DHNBP powder was dissolved into 1 mL DCM. Then, 500 μL EtOH was added into this DHNBP/DCM solution, resulting in a volume ratio of DCM to EtOH of 2:1. After shaking for some time, the well-mixed solution was dropped onto a glass substrate, which was then covered with a watch glass. DHNBP microwires were obtained as the solvents gradually evaporated. Additionally, branched microwires of DHNBP were fabricated using the same method with DCM to EtOH ratios adjusted to 1:2 and 1:4 for primary branched microwires and secondary branched microwires, respectively.

RESULTS AND DISCUSSION

DHNBP was designed based on a previously reported organic material (*E*)-3-(4-(dimethylamino)phenyl)-1-(2-hydroxyphenyl)-prop-2-en-1-one (DHMAC), which shows a red emission at 650 nm because of the excited state intramolecular proton transfer process and intramolecular donor-acceptor interaction [52,53]. We combined two DHMAC molecules to elongate the π-conjugation length, which leads to a narrowing of the highest occupied molecular orbital-lowest unoccupied molecular orbital (HOMO-LUMO) energy gap and results in further red shift emission (Fig. 1b, c) [54,55]. A larger π-conjugated system can strengthen the intermolecular π-π interaction, which is helpful for the formation of uniaxially oriented molecular crystals [56]. Uniaxially oriented molecular crystals with organic molecules packed into the same molecular conformation and orientation always have high anisotropic refractive indices and direct the propagation of the emitting light in a preferential direction, leading to excellent waveguide performance and high polarized light emission [57,58]. However, achieving uniaxially oriented molecular crystals remains challenging because organic molecules always have multiple conformations and various interactions in crystals [59–61]. The centrosymmetric molecular structure of DHNBP was adopted to balance intermolecular interactions and achieve a uniaxially oriented molecular crystal.

DHNBP was synthesized *via* the six-step synthesis route shown in Scheme S1. Compound **3** was synthesized according to previously reported procedures [62], which is proceeded by a two-step acetylation reaction to form Compound **5**. After demethylation by BBr_3, Compound **6** can be obtained. Finally, DHNBP was synthesized through the Claisen-Schmidt condensation reaction of Compound **6** and 4-(dimethylamino)-benzaldehyde (Compound **7**). Next, the photophysical properties of DHNBP were studied using ultraviolet-visible (UV-vis) absorption spectroscopy and PL spectroscopy in DCM solution (Fig. S5). The absorption and PL maxima occur at 501 and 652 nm, respectively. A large Stokes shift of 150 nm can be observed; this shift is beneficial for avoiding the self-reabsorption effect in optical applications.

Single crystals of DHNBP were prepared by slowly vaporizing a mixed solution of DCM and EtOH (6:1, *v*/*v*) at room temperature. When excited by a 375-nm laser, bulk DHNBP crystals showed a red to NIR fluorescence emission with a wavelength ranging from 600 to 900 nm and a maximum emission wavelength of 730 nm (Fig. S5). The molecular packing mode was investigated using single-crystal XRD, the results of which are shown in Fig. S6 and Table S1. DHNBP crystals belong to the triclinic system and space group $P\bar{1}$ with cell parameters of a = 5.1154(4) Å, b = 11.8779(9) Å, c = 12.1137(10) Å, α = 116.915(4)°, β = 102.128(2)°, and γ = 92.562(3)°. Different from the edge-to-face packing mode of DHMAC (left in Fig. 1b), all DHNBP molecules are packed with identical conformation and orientation along the a axis in the crystal, exhibiting regular uniaxially oriented packing (right in Fig. 1b and Fig. S7). To the best of our knowledge, this type of face-to-face packing always prefers to form a one-dimensional morphology in the crystal growth process.

Microcrystals were fabricated by a facial drop-drying method. First, DHNBP was completely dissolved in DCM at room tem-

perature with a concentration of 1.0 mmol L^{-1}. Then, 0.2 mL DHNBP solution in DCM was added into 0.1 mL EtOH and mixed by a brief and strong shake of the mixture. The mixed solution was then immediately dropped onto a glass substrate. After the solvents evaporated, microwires were finally obtained, as shown in Fig. S8 (bright-field microscopy image). A single microwire with a length of 44 μm is shown in Fig. 1c. The optical waveguide behavior of DHNBP microwires was studied based on this single wire, using a laser microspectral analysis system (Fig. S9). When the microwire was excited at different positions using a 375-nm laser beam, the relative PL spectra at the tip position were collected, as shown in Fig. 1d. The ratio between the PL intensity at 740 nm (maximum intensity) at the tip and the excitation position (I_{tip}/I_{body}) had a nonlinear relationship with the distance of the tip and excitation position (D), which could be fitted by a single-exponential decay function: $I_{tip}/I_{body} = A\exp(-RD)$ (inset in Fig. 1d). The optical-loss coefficient R was calculated to be 0.016 dB μm^{-1}, suggesting excellent optical waveguide performance in the DHNBP microwires, which is essential for integrated photonic applications.

Interestingly, the PL spectra at the tip position of the DHNBP microwires show a series of sharp fluorescence resonance peaks that indicate an optical cavity effect. For further investigation, PL spectra of microwires with different lengths at the tip position were detected. Fig. 1e shows the PL spectrum of a selected microwire with a length of 17.5 μm. Resonance peaks are very obvious in this spectrum, with the space between the individual spectral peaks ($\Delta\lambda$) measured to be 4.0 nm at a wavelength of 725 nm. The $\Delta\lambda$ was found to decrease with microwire length (L) and increase with fluorescence wavelength (PL spectra for microwires of different lengths can be seen in Fig. S10). This trend showed a good linear relationship between $\Delta\lambda$ at 725 nm and $1/L$, conforming to typical characteristics of a Fabry-Perot (FP) resonator (inset of Fig. 1e) [63]. Significantly, the FP cavity effect suggests the excellent light confinement property of DHNBP microwires, which is essential for the propagation of photon signals in optical circuits. Next, the polarization property of the microwires was studied. A strong polarization phenomenon in the emission light at the tip position of a selected microwire was observed, which is consistent with the distribution function of the linear polarization (Fig. S11). The data can be well fitted by a cosine quadratic function ($\cos^2\theta$), which is a characteristic of polarized emission from uniaxially oriented molecular crystals [62].

After obtaining DHNBP microwires with excellent optical properties, we tried to fabricate integrated structures for optical logic operation. According to our previous work [23], a synthesis method for branched homostructures was proposed and is shown in Fig. 2a. DHNBP can be dissolved in DCM at the concentration of 1 mmol L^{-1}, but almost insoluble in EtOH. So, DCM was used as a good solvent and EtOH was used as a poor solvent. Under good-solvent-dominant conditions, like

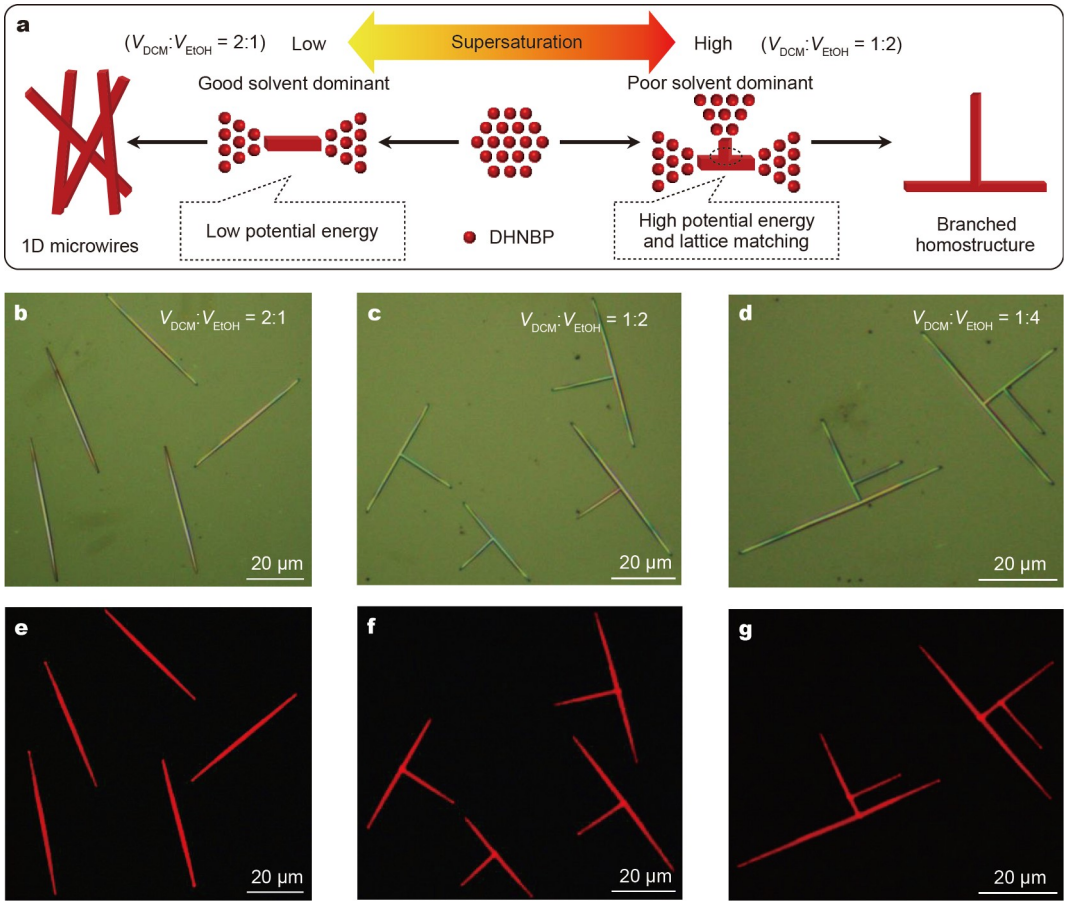

Figure 2 Fabrication of DHNBP microwires. (a) Schematic of the growth mechanism of individual and branched microwires. Bright-field microscopy images of (b) individual microwires, (c) primary branched microwires, and (d) secondary branched microwires. PL microscopy images of (e) individual microwires, (f) primary branched microwires and (g) secondary branched microwires.

V_{DCM}:V_{EtOH} = 2:1, the supersaturation of the solution is relatively low. Epitaxial growth in the side direction, which should get over the energy barrier, could not occur because of the low growth potential energy [64]. Therefore, only individual microwires can be formed (Fig. 2b, c, and Fig. S8). On the contrary, at poor-solvent-dominant conditions, like V_{DCM}:V_{EtOH} = 1:2, the supersaturation of the solution is relatively high. Meanwhile, the growth potential energy is correspondingly high, which helps overcome the energy barrier of the epitaxial growth in the side direction. As a result, branched structures may form on the basis of lattice matching. Fortunately, when we increased the volume ratio of EtOH in the above drop-drying method, branched microwires were formed. As shown in Fig. 2d, e, and Fig. S12, primary branched microwires were formed at a large scale when V_{DCM}:V_{EtOH} = 1:2. Excitingly, when we further increased the volume ratio of EtOH to V_{DCM}:V_{EtOH} = 1:4, a secondary branch was selectively grown from the primary branch to form a totally new organic homostructure (secondary branched microwire), which had not yet been reported (Fig. 2f, g, and Fig. S13). When the volume ratio of EtOH was further increased to V_{DCM}:V_{EtOH} = 1:6 or V_{DCM}:V_{EtOH} = 1:8, more complex multilevel branched structures formed. However, in these cases, the crystals start to bend, suggesting crystalline defects because of the dislocation of crystal lattice during the high-speed growth process (Fig. S14).

To illustrate the growth mechanism of the branched microwires, XRD was performed on both individual and branched microwires. The results showed that both microwire types have the same crystal structure according to the same characteristic peaks of (01-1) and (020) crystal planes (Fig. S15). From the SEM images of primary and secondary branched microwires (Fig. 3a, b, and Fig. S16), we can see that the branch and trunk of the wires are smoothly connected at an angle of 92.6°, which fits the γ angle of the unit cell perfectly. This phenomenon was also verified by the TEM images of the branched structures (Fig. S17). From the selected area electron diffraction (SAED) patterns of individual and branched microwires, we can clearly find that the trunk and branch both grow along the [100] crystal direction (Fig. S17). Fig. 3c shows a schematic of the junction position of the DHNBP microwires. The growth of the microwires should be along the *a* axis direction according to the molecular packing mode for uniaxially oriented molecular crystals and the SAED patterns. This is also consistent with the calculation result for the growth morphology obtained using the material studio software (Fig. 3d). Therefore, we can speculate that the *a* axis direction of the branch should be the same as the *b* axis direction of the backbone, such that the angle is the same as the γ angle. In addition, the growth of the crystal can also be demonstrated by the attachment energy of the crystal planes. The calculated result from the Materials Studio package shows that the (100) crystal plane has very high attachment energy (approximately −74.8 kJ mol^{-1}) while the attachment energies of the (010) and (01-1) planes are relatively low (−18.3 and −20.8 kJ mol^{-1}, respectively, Table S2). This means that the packing speed of the (100) plane is much faster than those of the other two planes, resulting in a large exposure area of the (010) and (01-1) planes, which is consistent with the XRD results. We now estimate that the connected planes at the junction position should be at the (010) plane of the trunk structure and the (100) plane of the branch structure. As shown in Fig. 3e, the interplanar spacing of the (010) plane is 20.9 Å and the interplanar spacing of the (100) plane is 9.9 Å. The mismatching rate was

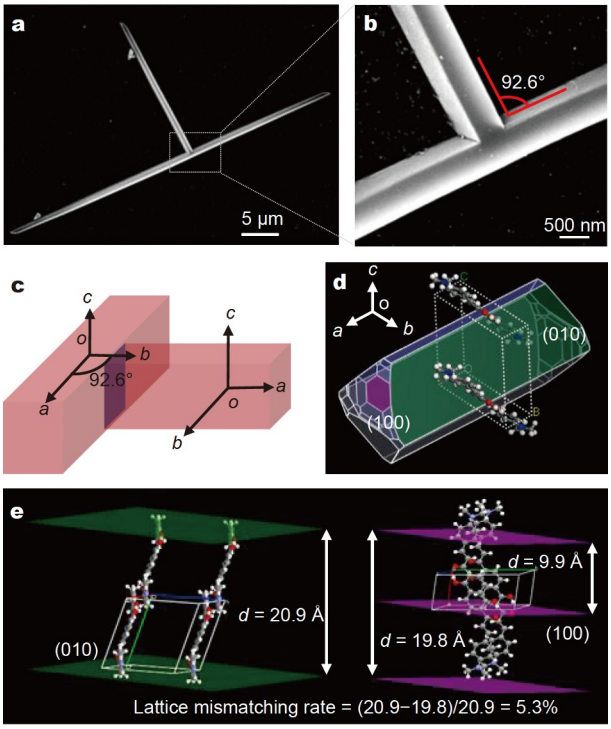

Figure 3 Growth mechanism study of the branched microwires. (a) Scanning electron microscopy (SEM) image of a primary microwire. (b) Partial magnification of the SEM image at the junction position. (c) Schematic of trunk and branch orientations at the junction position. The purple rectangle shows the junction between the *a*, *c*-plane of the trunk and the *b*, *c*-plane of the branch. (d) Simulated growth morphology of DHNBP. (e) Molecular packing and interplanar spacing of (010) and (100) planes.

calculated to be 5.3%, suggesting good lattice matching between the (010) and (100) planes of the DHNBP microwires and contributing to the growth of branched structures. On the basis of the above analysis, synthesis of branched microwires can be achieved by modulation of the supersaturation of the mixed solution.

To reveal the optical signal propagation behavior of our branched DHNBP microwires, optical waveguide properties of a selected primary branched microwire were studied. Fig. 4a shows an optical microscope image of the branched microwire. First, we excited the O position of the homostructure with a 375-nm laser beam and collected the out-coupled emission spectra at the tip positions A, B, and C, as shown in Fig. 4b. Interestingly, resonance peaks were obvious in all the spectra (Fig. 4e). For the A and B position spectra, the values of $\Delta\lambda$ are both 2.4 nm, while that of the C position is 4.8 nm at a wavelength of 730 nm. This suggests that the trunk and branch can be FP-type resonators with almost no mutual interference between them. Therefore, we have integrated two optical resonators with different directions, which provide a new platform for the investigation of photonics in microcavities. Next, we focused the laser beam on two sides of the junction, with $d(E_1O_1) = d(E_2O_2)$ and collected PL spectra at positions C_1 and C_2 (Fig. 4c, d). The different intensities of the output light at positions C_1 and C_2 show the asymmetrical optical waveguide property of the junction (Fig. 4f). This phenomenon can account for the different levels of reflection of input-light at the junction position because of the different angles, ∠AOC and ∠BOC [44]. This asymmetrical optical

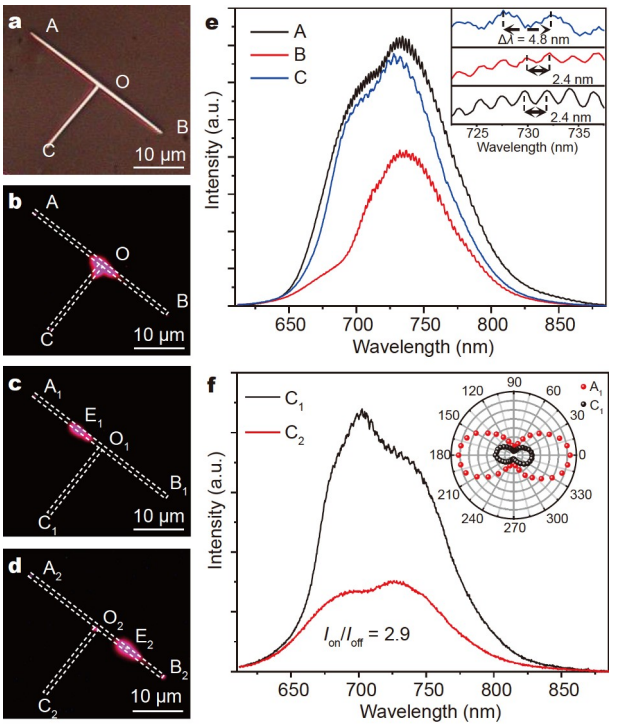

Figure 4 Optical properties of primary branched microwires. (a) Bright-field microscopy image of a typical primary branched microwire. (b–d) PL microscopy images of the primary branched microwire when excited at different positions with a focused laser beam (λ = 375 nm). (e) PL spectra at tip positions A, B, and C when excited at the O position. Inset: partial magnification at the 720–740 nm position of the PL spectra at A, B, and C positions. (f) PL spectra at the C_1 and C_2 positions when excited at E_1 and E_2 positions, respectively. Inset: polar image of the peak intensities at A_1 and C_1 positions when excited at the E_1 position.

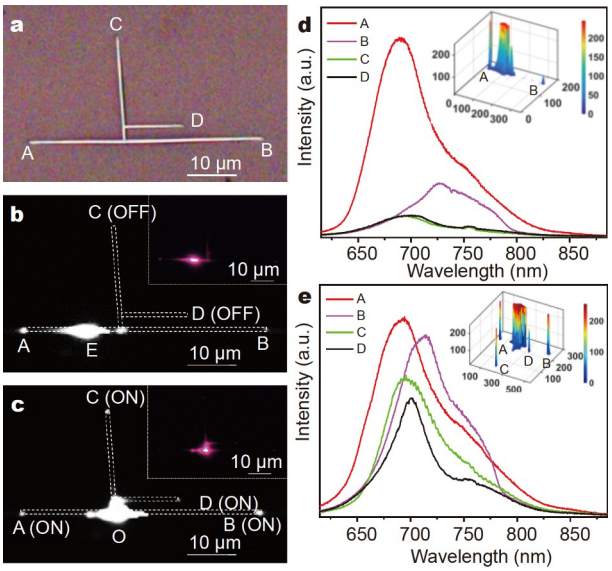

Figure 5 Optical properties of secondary branched microwires. (a) Bright-field microscopy image of a typical secondary branched microwire. (b, c) Far-field PL microscopy images of the primary branched microwire when excited at different positions with a focused laser beam (λ = 375 nm). Inset: corresponding PL microscopy images. PL spectra at the tip positions A, B, C, and D when excited at the (d) E position (inset: corresponding spatially resolved peak intensities), and (e) O position (inset: corresponding spatially resolved peak intensities).

waveguide behavior could be used in an optical logic gate, which is an important component in integrated optical circuits [65,66]. The ON/OFF ratio of this optical logic gate was calculated to be 2.9, which is approaching a useful level. The more interesting thing is that the out-coupling light at the C position is also polarized. When the E_1 position was excited by the laser beam, the polarization direction of the output light at the C_1 and A_1 positions was the same and depended on the polarization direction of the output light at the A_1 position (the inset in Fig. 4f). This phenomenon indicates that polarized light can be transmitted in the branched microwire, which can lead to stronger information transferability.

More impressively, a secondary branched microwire was selected to further explore the photonic performance of the DHNBP branched homostructures. As shown in Fig. 5a, the secondary branched microwire has four tips that represent four out-coupling positions: A, B, C, and D. A variety of combinations of the out-coupling signals can be achieved when exciting the homostructure at a specified position. Here, two examples are presented. Fig. 5b shows an image generated by a CCD, in which NIR signals are also displayed (the inset is the PL microscope image). When excited at the E position, four different optical signals could be collected, in which the signal at the A position was relatively strong, and the signal at the B position was much weaker. At positions C and D, the signals were extremely weak and could be regarded as a closed channel. Therefore, a combined signal of A(STRONG)-B(WEAK)-C(OFF)-D(OFF) was formed, as shown in Fig. 5d and the inset. Fig. 5c and its corresponding inset show images when excited at the O position; the bright spots at all tips are very clear, except for that at the D spot, which is a little weaker. From the spectra, it can be seen that the PL intensities of all tips are similar and can be defined as an all-ON signal of A(ON)-B(ON)-C(ON)-D(ON) (Fig. 5e and the inset). Thus, the secondary branched microwires could potentially be used as optical signal processors in integrated photonic circuits.

CONCLUSIONS

In summary, NIR emissive single and multilevel branched organic microwires with different integration levels were fabricated successfully *via* the self-assembly method based on a new organic semiconductor material: DHNBP. Individual microwires could be obtained using good-solvent-dominant conditions, and branched structures could be prepared at poor-solvent-dominant conditions, benefiting from lattice matching of the (100) and (010) crystal planes and high growth potential energy induced by high supersaturation. DHNBP crystals showed a uniaxially oriented molecular packing mode, which endows the microwires with outstanding optical waveguide properties and a low optical-loss coefficient of 0.016 dB μm^{-1}. For the primary branched microwires, the trunk and branch structures work as resonators with negligible mutual interference. Furthermore, an asymmetric waveguide was observed, which provides the opportunity to apply the wires in ON/OFF optical logic gates. The ability to transmit polarized light in the branched structure was also observed. For higher integrated secondary branched microwires, we demonstrated optical signal processors that can generate different combined signals composed of signals at four tip positions. We believe that our fabricated multilevel branched organic microwires will potentially boost the development of

integrated photonic devices.

Received 3 July 2021; accepted 16 September 2021; published online 29 October 2021

1 Horowitz M, Yang CKK, Sidiropoulos S. High-speed electrical signaling: Overview and limitations. IEEE Micro, 1998, 18: 12–24
2 Caulfield HJ, Dolev S. Why future supercomputing requires optics. Nat Photon, 2010, 4: 261–263
3 Engheta N. Circuits with light at nanoscales: Optical nanocircuits inspired by metamaterials. Science, 2007, 317: 1698–1702
4 Kirchain R, Kimerling L. A roadmap for nanophotonics. Nat Photon, 2007, 1: 303–305
5 Bogaerts W, Pérez D, Capmany J, *et al.* Programmable photonic circuits. Nature, 2020, 586: 207–216
6 Duan X, Huang Y, Cui Y, *et al.* Indium phosphide nanowires as building blocks for nanoscale electronic and optoelectronic devices. Nature, 2001, 409: 66–69
7 Bao J, Zimmler MA, Capasso F, *et al.* Broadband ZnO single-nanowire light-emitting diode. Nano Lett, 2006, 6: 1719–1722
8 Grosshans F, Van Assche G, Wenger J, *et al.* Quantum key distribution using Gaussian-modulated coherent states. Nature, 2003, 421: 238–241
9 Zhang Q, Zhu X, Li Y, *et al.* Nanolaser arrays based on individual waved CdS nanoribbons. Laser Photonics Rev, 2016, 10: 458–464
10 Law M, Sirbuly DJ, Johnson JC, *et al.* Nanoribbon waveguides for subwavelength photonics integration. Science, 2004, 305: 1269–1273
11 Cui Y, Zhong Z, Wang D, *et al.* High performance silicon nanowire field effect transistors. Nano Lett, 2003, 3: 149–152
12 Colinge JP, Lee CW, Afzalian A, *et al.* Nanowire transistors without junctions. Nat Nanotech, 2010, 5: 225–229
13 Yan R, Gargas D, Yang P. Nanowire photonics. Nat Photon, 2009, 3: 569–576
14 Piccione B, Cho CH, van Vugt LK, *et al.* All-optical active switching in individual semiconductor nanowires. Nat Nanotech, 2012, 7: 640–645
15 Bai S, Wu W, Qin Y, *et al.* High-performance integrated ZnO nanowire UV sensors on rigid and flexible substrates. Adv Funct Mater, 2011, 21: 4464–4469
16 Park KS, Lee KS, Kang CM, *et al.* Cross-stacked single-crystal organic nanowire p-n nanojunction arrays by nanotransfer printing. Nano Lett, 2015, 15: 289–293
17 Sirbuly DJ, Law M, Pauzauskie P, *et al.* Optical routing and sensing with nanowire assemblies. Proc Natl Acad Sci USA, 2005, 102: 7800–7805
18 Wei H, Wang Z, Tian X, *et al.* Cascaded logic gates in nanophotonic plasmon networks. Nat Commun, 2011, 2: 387
19 Clark J, Lanzani G. Organic photonics for communications. Nat Photon, 2010, 4: 438–446
20 Liu CF, Liu X, Lai WY, *et al.* Organic light-emitting field-effect transistors: Device geometries and fabrication techniques. Adv Mater, 2018, 30: 1802466
21 Liu J, Zhang H, Dong H, *et al.* High mobility emissive organic semiconductor. Nat Commun, 2015, 6: 10032
22 Li J, Zhou K, Liu J, *et al.* Aromatic extension at 2,6-positions of anthracene toward an elegant strategy for organic semiconductors with efficient charge transport and strong solid state emission. J Am Chem Soc, 2017, 139: 17261–17264
23 Zhuo MP, Tao YC, Wang XD, *et al.* 2D organic photonics: An asymmetric optical waveguide in self-assembled halogen-bonded cocrystals. Angew Chem Int Ed, 2018, 57: 11300–11304
24 Chen S, Zhuo MP, Wang XD, *et al.* Optical waveguides based on one-dimensional organic crystals. PhotoniX, 2021, 2: 2
25 Jiang Y, Liu YY, Liu X, *et al.* Organic solid-state lasers: A materials view and future development. Chem Soc Rev, 2020, 49: 5885–5944
26 Wu JJ, Gao H, Lai R, *et al.* Near-infrared organic single-crystal nanolaser arrays activated by excited-state intramolecular proton transfer. Matter, 2020, 2: 1233–1243
27 Wu JJ, Zhuo MP, Lai R, *et al.* Cascaded excited-state intramolecular proton transfer towards near-infrared organic lasers beyond 850 nm. Angew Chem Int Ed, 2021, 60: 9114–9119
28 Jiang Y, Li KF, Gao K, *et al.* Frequency-upconverted stimulated emission by up to six-photon excitation from highly extended spiro-fused ladder-type oligo(*p*-phenylene)s. Angew Chem Int Ed, 2021, 60: 10007–10015
29 Zhuo MP, Wu JJ, Wang XD, *et al.* Hierarchical self-assembly of organic heterostructure nanowires. Nat Commun, 2019, 10: 3839
30 Lei Y, Sun Y, Zhang Y, *et al.* Complex assembly from planar and twisted π-conjugated molecules towards alloy helices and core-shell structures. Nat Commun, 2018, 9: 4358
31 Lin J, Liu B, Yu M, *et al.* Ultrastable supramolecular self-encapsulated wide-bandgap conjugated polymers for large-area and flexible electroluminescent devices. Adv Mater, 2019, 31: 1804811
32 Zhuo MP, Fei XY, Tao YC, *et al. In situ* construction of one-dimensional component-interchange organic core/shell microrods for multicolor continuous-variable optical waveguide. ACS Appl Mater Interfaces, 2019, 11: 5298–5305
33 Liu Y, Peng C, Xiong W, *et al.* Two-dimensional seeded self-assembly of a complex hierarchical perylene-based heterostructure. Angew Chem Int Ed, 2017, 56: 11380–11384
34 Yang C, Gu L, Ma C, *et al.* Controllable co-assembly of organic micro/nano heterostructures from fluorescent and phosphorescent molecules for dual anti-counterfeiting. Mater Horiz, 2019, 6: 984–989
35 Pan ML, Wang C, Zhuo MP, *et al.* Sequential self-assembly of organic heterostructured architectures composed of low-dimensional microcrystals. ACS Mater Lett, 2020, 2: 658–664
36 Zhuo MP, He GP, Wang XD, *et al.* Organic superstructure microwires with hierarchical spatial organisation. Nat Commun, 2021, 12: 2252
37 Zhuo MP, He GP, Yuan Y, *et al.* Super-stacking self-assembly of organic topological heterostructures. CCS Chem, 2021, 3: 413–424
38 Jiang X, Tian B, Xiang J, *et al.* Rational growth of branched nanowire heterostructures with synthetically encoded properties and function. Proc Natl Acad Sci USA, 2011, 108: 12212–12216
39 Zheng JY, Yan Y, Wang X, *et al.* Wire-on-wire growth of fluorescent organic heterojunctions. J Am Chem Soc, 2012, 134: 2880–2883
40 Li YJ, Yan Y, Zhang C, *et al.* Embedded branch-like organic/metal nanowire heterostructures: Liquid-phase synthesis, efficient photon-plasmon coupling, and optical signal manipulation. Adv Mater, 2013, 25: 2784–2788
41 Yao W, Han G, Huang F, *et al.* "H"-like organic nanowire heterojunctions constructed from cooperative molecular assembly for photonic applications. Adv Sci, 2015, 2: 1500130
42 Zhang Y, Liao Q, Wang X, *et al.* Lattice-matched epitaxial growth of organic heterostructures for integrated optoelectronic application. Angew Chem Int Ed, 2017, 56: 3616–3620
43 Li ZZ, Tao YC, Wang XD, *et al.* Organic nanophotonics: Self-assembled single-crystalline homo-/heterostructures for optical waveguides. ACS Photonics, 2018, 5: 3763–3771
44 Tao YC, Peng S, Wang XD, *et al.* Sequential self-assembly of 1D branched organic homostructures with optical logic gate function. Adv Funct Mater, 2018, 28: 1804915
45 Todoroki S, Sakaguchi S, Sugii K. Evaluation of optical glasses for low-loss fibers: Optical attenuation and fiber drawing ability. Jpn J Appl Phys, 1995, 34: 3128–3133
46 Harrison MT, Kershaw SV, Burt MG, *et al.* Colloidal nanocrystals for telecommunications. Complete coverage of the low-loss fiber windows by mercury telluride quantum dot. Pure Appl Chem, 2000, 72: 295–307
47 Weissleder R, Tung CH, Mahmood U, *et al. In vivo* imaging of tumors with protease-activated near-infrared fluorescent probes. Nat Biotechnol, 1999, 17: 375–378
48 Xu W, Wang D, Tang BZ. NIR-II AIEgens: A win-win integration towards bioapplications. Angew Chem Int Ed, 2021, 60: 7476–7487
49 Schanze KS, Reynolds JR, Boncella JM, *et al.* Near-infrared organic light emitting diodes. Synth Met, 2003, 137: 1013–1014
50 Zampetti A, Minotto A, Cacialli F. Near-infrared (NIR) organic light-emitting diodes (OLEDs): Challenges and opportunities. Adv Funct Mater, 2019, 29: 1807623
51 Williams EL, Li J, Jabbour GE. Organic light-emitting diodes having exclusive near-infrared electrophosphorescence. Appl Phys Lett, 2006, 89: 083506

52 Wang X, Liao Q, Lu X, *et al.* Shape-engineering of self-assembled organic single microcrystal as optical microresonator for laser applications. Sci Rep, 2014, 4: 7011
53 Zhang W, Yan Y, Gu J, *et al.* Low-threshold wavelength-switchable organic nanowire lasers based on excited-state intramolecular proton transfer. Angew Chem Int Ed, 2015, 54: 7125–7129
54 Qian G, Wang ZY. Near-infrared organic compounds and emerging applications. Chem Asian J, 2010, 5: 1006–1029
55 Aoki R, Komatsu R, Goushi K, *et al.* Realizing near-infrared laser dyes through a shift in excited-state absorption. Adv Opt Mater, 2021, 9: 2001947
56 Varghese S, Yoon SJ, Calzado EM, *et al.* Stimulated resonance Raman scattering and laser oscillation in highly emissive distyrylbenzene-based molecular crystals. Adv Mater, 2012, 24: 6473–6478
57 Shimizu K, Mori Y, Hotta S. Laser oscillation from hexagonal crystals of a thiophene/phenylene co-oligomer. J Appl Phys, 2006, 99: 063505
58 Yamao T, Okuda Y, Makino Y, *et al.* Dispersion of the refractive indices of thiophene/phenylene co-oligomer single crystals. J Appl Phys, 2011, 110: 053113
59 Li Y, Shen F, Wang H, *et al.* Supramolecular network conducting the formation of uniaxially oriented molecular crystal of cyano substituted oligo(*p*-phenylene vinylene) and its amplified spontaneous emission (ASE) behavior. Chem Mater, 2008, 20: 7312–7318
60 Wang H, Li F, Ravia I, *et al.* Cyano-substituted oligo(*p*-phenylene vinylene) single crystals: A promising laser material. Adv Funct Mater, 2011, 21: 3770–3777
61 Chen J, Ma S, Zhang J, *et al.* Low-loss optical waveguide and highly polarized emission in a uniaxially oriented molecular crystal based on 9,10-distyrylanthracene derivatives. ACS Photonics, 2015, 2: 313–318
62 Wu X, Zhang P, Yang Z, *et al.* Polymerization of phenylacetylenes by binuclear rhodium catalysts with different *para*-binucleating phenoxyiminato linkages. Polym Chem, 2019, 10: 4163–4172
63 Wang X, Liao Q, Xu Z, *et al.* Exciton-polaritons with size-tunable coupling strengths in self-assembled organic microresonators. ACS Photonics, 2014, 1: 413–420
64 Desiraju GR. Cryptic crystallography. Nat Mater, 2002, 1: 77–79
65 Yao W, Yan Y, Xue L, *et al.* Controlling the structures and photonic properties of organic nanomaterials by molecular design. Angew Chem Int Ed, 2013, 52: 8713–8717
66 Lv Y, Xu FF, Wang K, *et al.* Loss compensation of surface plasmon polaritons in organic/metal nanowire heterostructures toward photonic logic processing. Sci China Mater, 2020, 63: 1464–1471

Acknowledgements This work was financially supported by the National Natural Science Foundation of China (21971185 and 51821002), China Postdoctoral Science Foundation (2020M681707), the Collaborative Innovation Center of Suzhou Nano Science and Technology (CIC-Nano), and the "111" Project of the State Administration of Foreign Experts Affairs of China.

Author contributions Wang XD and Liao LS designed the experiments. Yan CC and Yang WY synthesized and characterized the organic molecules. Yan CC, Wu JJ, Yang WY, Chen S, and Lv Q conducted the structural characterizations of organic microwires. Yan CC, Wu JJ and Yang WY operated the optical characterizations. Yan CC, Wang XD, and Liao LS interpreted the results and wrote the paper. All authors discussed the results and commented on the manuscript.

Conflict of interest The authors declare that they have no conflict of interest.

Supplementary information Experimental details and supporting data are available in the online version of the paper.

Chang-Cun Yan received his PhD degree from the College of Chemistry, Nankai University, in 2017. He is currently a postdoctoral research fellow at the Institute of Functional Nano & Soft Materials (FUNSOM) of Soochow University under the guidance of Prof. Liang-Sheng Liao. His current research focuses on the design, synthesis, and application of organic semiconductor materials and organic photonics.

Xue-Dong Wang is a professor at the Institute of FUNSOM of Soochow University. He received his PhD degree in physical chemistry at the Institute of Chemistry, Chinese Academy of Sciences, in 2016. His research focuses on the fine synthesis of organic micro/nanocrystals and organic photonics, including organic solid-state lasers and optical waveguides.

Liang-Sheng Liao received his PhD degree in physics from Nanjing University, China. After working at Eastman Kodak Company as a senior research scientist from 2000 to 2009, he joined the Institute of FUNSOM, Soochow University as a full professor. His current research interests include materials and architectures of OLEDs as well as organic lasers, quantum-dot LEDs, organic solar cells, and perovskite solar cells.

具有近红外区域光信号处理功能的多级枝权结构有机微米线的精确制备

闫长存[1], 吴俊杰[1], 杨婉莹[1], 陈松[1], 吕强[1], 王雪东[1*], 廖良生[1,2*]

摘要 复杂的多级微纳米结构是集成光电子器件的基本组成部分，然而其精确制备依然面临着巨大的挑战. 本文基于有机近红外发光材料DHNBP，利用简易的溶液自组装方法首次成功制备了多级枝权型有机微米线晶体. 在不同的制备条件下，该类多级枝权结构的集成度也会随之变化. 生长机理研究表明(100)晶面和(010)晶面完美的晶格匹配(晶格失配率低至5.3%)起到了至关重要的作用. 得益于晶体中分子的单向排列模式，无论是单一微米线还是多级枝权型微米线都具有优异的光学性质. 另外，本文进一步展示了该多级枝权型微米线作为光学逻辑门及光信号处理器的应用. 本文所展示的多级枝权型有机微纳晶体有可能会进一步推动集成光电子器件的发展.

